Solid propellants burning enhancement using foil embedding method

H. G. Darabkhanid and N. S. Mehdizadeh
Aerospace Engineering Department
Amirkabir University of Technology
Centre of Excellence in Computational Aerospace Engineering
Tehran, Iran

ABSTRACT

The method of metal embedding is widely employed in solid propellant motors with end-burning configuration, thereby significantly improving the burning rate of the propellants. In this study, the cylindrical foil embedding method is applied to double-base solid propellant, as a new method, and the effects of the type and thickness of the foil on the burning surface, as well as the burning rate, are experimentally investigated. It is shown that by using the foil embedding method, the burning characteristics of solid propellants can be improved. Results have been compared to some available data. To the best of the author's knowledge there are no published data available on this method.

NOMENCLATURE

a	burning coefficient
A	cross-sectional area
A_T	throat area of the nozzle
c	specific heat
C^*	characteristic velocity
df	foil diameter
F	thrust
F_o	thrust for the case of end-burning
h	convection heat transfer coefficient
k	thermal conductivity
L	latent heat
l_f	overall length of the foil
m	mass of melted foil
n	pressure exponent in burning rate equation
P	pressure, foil perimeter
q, q''	heat flux
r_b	burning rate without foil
r_f	burning rate along the foil
S	burning surface
S_T	cross-sectional surface
T	temperature
u	velocity
v	velocity
V_r, V_z	velocity
w	velocity
Z	foil length
Z_c	part of the foil, in contact with the flue gas
Z_m	melting part of the foil

Greek letters

α	thermal diffusivity
θ	angle between the foil and the propellant surface
ρ	density
ρ_p	solid propellant density
σ	radiation heat transfer coefficient

Subscripts

b	bare
f	foil
g	gas

Paper No. 3247. Manuscript received 30 October 2007, revised version received 5 May 2008, second revised version received 30 July 2008, accepted 1 October 2008.

https://doi.org/10.1017/S0001924000002694 Published online by Cambridge University Press

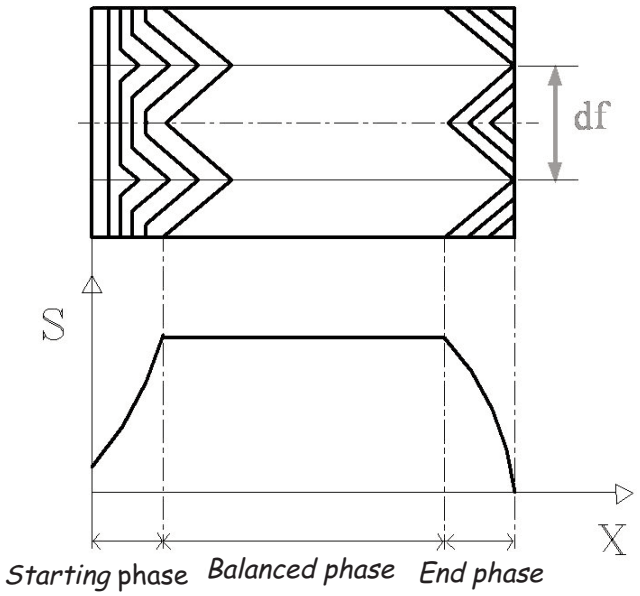


Figure 1. Burning phases for foil embedded solid propellant.

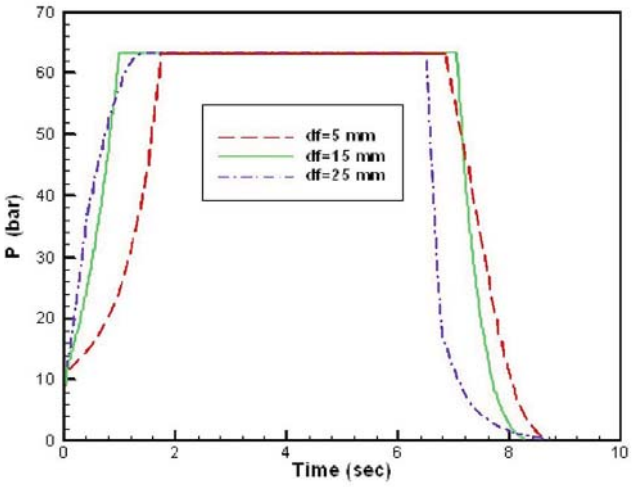


Figure 2. Pressure variation for foil embedded solid propellant (numerical data).

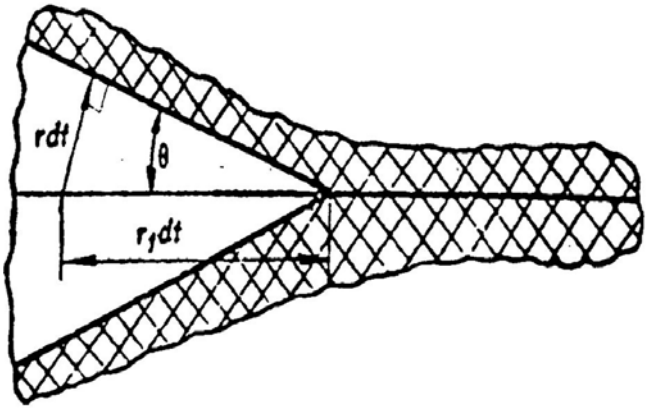


Figure 3. cross-section of burning surface, produced due to conning effect (half part of W-shape).

1.0 INTRODUCTION

For solid propellant motors, two types of grains are typically used: end-burned and internal-burned. Normally, burning time is high for end-burned grains, whereas burning time is greatly lower for internal-burned grains. It is generally not convenient to attain a suitable burning time by modifying the geometry of the solid propellant. One of the best ways for controlling the burning time is by employing the metal embedding method, using fibres, wires, or foils. In this research a novel cylindrical foil embedding technique is investigated experimentally.

Rumbel *et al* (1955) pioneered the use of embedded metallic wires to enhance solid-propellant burning rates. This database encompassed a wide range of pressure, wire diameter, and wire material (i.e. silver, aluminium, and copper). King (1991) presented a model for the burning of wire embedded propellants and compared the results with experimental data. Wang *et al* (1998) studied the effect of the quantity and the position of wires in solid propellants. Sahafiyan and Afshani (2005) presented a numerical method for burning rate calculation for a model solid propellant motor, embedded with three silver wires.

2.0 COMBUSTION LAWS

During the first step of end burning (labelled as 'starting phase', Fig. 1), the solid propellant burns with a burning rate of r_b. Afterwards, heat penetrates into the solid propellant through the metallic foil. When the solid propellant temperature reaches the auto-ignition value, the portion of the solid propellant, adjacent to the foil, burns, and then, combustion continues locally with a higher burning rate of r_f. Since r_f is greater than r_b, a 'conic W-shape' appears on the burning surface of the propellant (see Figs 1 and 7).

Accordingly, the burning surface increases and the burning time decreases. The W-shape moves down to the end of the solid propellant, where the 'end phase' starts. The steady part of burning, located between the start phase and end phase, is defined as the 'balanced phase' (see Fig. 1 in which *df* and *S* indicate the foil diameter and the burning surface in the propellant, respectively). The maximum burning time for this phase, can be achieved by embedding the foil at the mid diameter of the cylindrical solid propellant[3]. Figure 2 shows the effect of foil location on the pressure-time curve. These graphs are derived from a zero-dimensional computer program for internal ballistic of these types of motors[3]. Fig. 3 illustrates half part of the cross-section of the conic W-shape, established during the burning of foil embedded solid propellant.

In this figure:

$$\mathrm{Sin}\,\theta = \frac{r_b dt}{r_f dt} = \frac{r_b}{r_f} \qquad \ldots (1)$$

$$\theta = \mathrm{arcSin}\,\frac{r_b}{r_f} \qquad \ldots (2)$$

where θ indicates the angle between the foil and the propellant surface. The burning rate for the solid propellant without embedded foil is determined by $r_b = aP^n$ For the foil embedded solid propellant, burning rate can be estimated by $r_f = a_f P^{nf}$, in which a and a_f are the solid propellant burning coefficients, for end-burning and foil embedded burning cases, respectively. These coefficients depend on the solid propellant type, ambient temperature, and foil material. Moreover, n and n_f are the combustion indices for end-burning and foil embedded burning cases. Accordingly:

$$\mathrm{Sin}\theta = \frac{a}{a_f} P^{n-n_f} \qquad \ldots (3)$$

https://doi.org/10.1017/S0001924000002694 Published online by Cambridge University Press

Parameter N is defined as the ratio of combustion surface, in the foil embedded burning, to that of end-burning, without embedded foil (Equation (4)). By means of N, foil embedding effect on solid propellant burning rate, combustion chamber pressure, and combustion surface can be studied (4).

$$N = \frac{1}{\mathrm{Sin}\theta} \quad \ldots (4)$$

During the balanced phase a complete cone forms and the burning surface, S_f, is computed based on the cross-sectional surface of the solid propellant, S_T, as follows:

$$S_f = \frac{S_T}{\mathrm{Sin}\theta} \quad \ldots (5)$$

By using Equations (1), (4) and (5), it can be concluded that:

$$\frac{S_f}{S_T} = \frac{r_f}{r_b} = \bar{r}_f = N \quad \ldots (6)$$

Thrust for a foil embedded propellant motor, F_f, can be estimated by using Equation (7), based on the thrust of end-burning propellant motor, F_o, as follows:

$$\frac{F_f}{F_0} = N \quad \ldots (7)$$

In addition, combustion chamber pressure can be calculated based on the following Equation (3):

$$P = \left[c^* \rho_p a_f \left(\frac{S_T}{A_T} \right) \right]^{\frac{1}{1-n_f}} \quad \ldots (8)$$

where c^* is the characteristic velocity of the outgoing flue gas, ρ_P is the solid propellant density, and A_T is the throat area of the nozzle.

Heat affected zones and relevant coordinates for the foil embedded solid propellant modelling are shown in Fig. 4.

In this figure, important heat affected zones are:

- heat affected zone in solid propellant, where heat penetrates from hot flue gas into the solid propellant.
- heat affected zone in solid propellant, where heat penetrates from the hot metallic foil into the solid propellant.
- the interfering area of the above mentioned zones (interference zone), where heat penetrates, simultaneously, from the hot flue gas and the metallic foil into the solid propellant.
- reaction zone in hot flue gas, where the reactions are mainly take place.

It should be noted that volume of the heat affected zone in solid propellant, is negligible, and, it can be assumed that the solid propellant keeps its contact with the foil before transforming into the gas phase[5]. The hot flue gas moves perpendicularly from the burning surface, and continues its way along the metallic foil. Figure 4(b) explains the coordinates, according to which the heat transfer equations are derived.

3.0 HEAT TRANSFER EQUATIONS

3.1 Main assumptions

In order to derive the governing heat transfer equations the following assumptions are incorporated:

- heat transfer from foil to interference zone is negligible.
- longitudinal conduction heat transfer from foil to propellant is negligible with regard to the perpendicular conduction heat transfer.
- gas flow is inviscid, quasi-steady, and incompressible.
- foil is thermally thin.
- temperature distribution and flow pattern are two dimensional.
- propellant is homogeneous and isotopic.

3.2 Heat transfer in the foil

Considering the foil element, shown in Fig. 5, the heat transfer equation can be written as[3]:

$$k_f \frac{\partial T_f^{\,2}}{\partial z^2} + \frac{p}{A_f} q'' + \frac{q''}{r} = \rho c \frac{\partial T_f}{\partial t} \quad \ldots (9)$$

where k_f, p, q , A_f, and T_f are thermal conductivity of metallic foil, foil perimeter, heat flux, foil cross-sectional area, and foil temperature, respectively.

Thus, the heat flux from foil to the solid propellant can be calculated from (Fig. 6):

$$q'' = q''_p = k_f \left(\frac{\partial T_p(0,z,t)}{\partial r} \right) \quad \ldots (10)$$

where z_c is the part of the foil, which is in contact with the hot flue gas (bare part), and z_m is the melting part of the foil.

For the upper part of the foil ($0 \le z < z_C$), which is in contact with the hot gas, heat flux for the foil can be written as:

$$q'' = h(T_g - T_f) + \sigma F(T_g^{\,4} - T_f^{\,4}) \quad \ldots (11)$$

Since the foil is located in the middle of the propellant, the burning surfaces on the both sides are identical, and it can be assumed that $h_3 = h_4$, and then $q''_3 = q''_4$.

The initial condition is considered as[1]:

$$T_f(z,0) = T_i \qquad if: \ 0 \le z \le l_f \quad \ldots (12)$$

where l_f is the overall length of the foil. If the foil melting temperature is higher than the flue gas temperature, then the bare foil will resist and remain in its position, and the boundary condition becomes:

$$k_f \left(\frac{\partial T_f(0,t)}{\partial z} \right) = q''(0,t) \quad \ldots (13)$$

If the foil melting temperature is lower than the gas temperature, which is usually the case, then the bare foil will melt and the boundary condition is modified, as:

$$q_1 + q_3 + q_4 - q_2 - q_L = 0 \quad \ldots (14)$$

If we assume $q_3 = q_4$ then the heat transfer equation can be derived as:

$$q'' A_m + k_f A_f \frac{\partial T}{\partial z} - \frac{\Delta m}{\Delta t} L = 0 \quad \ldots (15)$$

where L is the latent heat, A_m is the melting surface of the foil, and m indicates the mass of melted foil.

Considering $\Delta m = 2\rho\pi r dr dz$ and foil melting rate as $S = \Delta z/\Delta t$, then:

$$A_f k_f \frac{\partial T_f(z_m,t)}{\partial z} - A_f . \rho_f . L . S = A_m q''(z_m,t) \quad \ldots (16)$$

https://doi.org/10.1017/S0001924000002694 Published online by Cambridge University Press

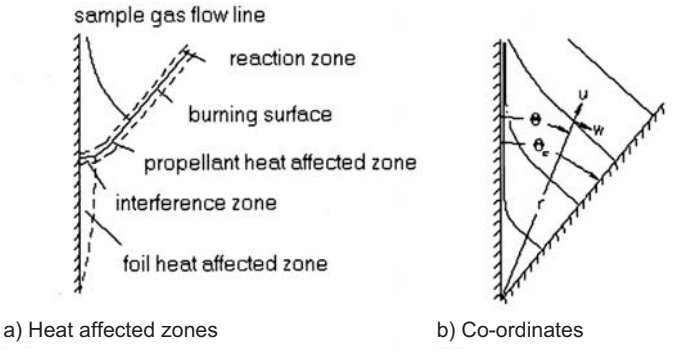


Figure 4. Heat affected zones and co-ordinates.

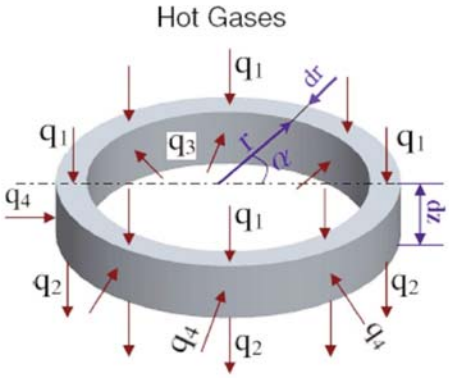


Figure 5. Foil element.

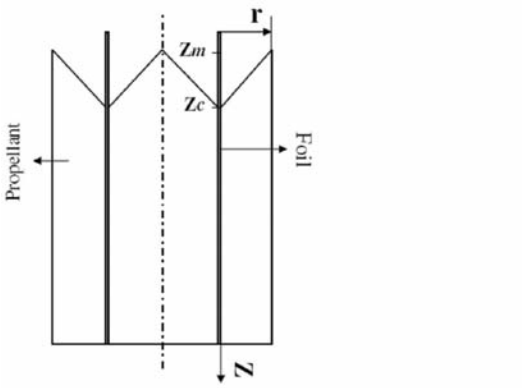


Figure 6. Co-ordinates of the foil in propellant.



Figure 7. cross-sections of burned propellant, embedded with Al and Cu foils.

3.3 Heat transfer from foil to propellant

The equation, describing heat transfer from the foil to the propellant, is:

$$\dot{q}_1 - \dot{q}_2 = mc\frac{\partial T}{\partial t} \qquad \ldots (17)$$

where $\dot{q}_1$ indicates the rate of heat transfer from the foil to propellant, and q_2 is the rate of outgoing heat transfer from the propellant element. Considering $\alpha_p = k/\rho c$ and using heat transfer equations, we arrive at:

$$\frac{\partial T_p}{\partial t} = \alpha_p\left(\frac{\partial^2 T_p}{\partial r^2} + \frac{1}{r}\frac{\partial T_p}{\partial r}\right) \qquad \ldots (18)$$

Moreover, initial and boundary conditions are:

$$T_p(r,z,0) = T_i \qquad if:\ 0 \le r,\ \ z_c \le z \qquad \ldots (19)$$

$$T_p(\infty,z,t) = T_i, \qquad T_p(r,z,t) = T_f(z,t) \qquad \ldots (20)$$

3.4 Convection heat transfer to foil

In order to derive the convection heat transfer rate, from hot flue gas to the foil, heat transfer coefficient for the flow field, shown in Fig. 4, has to be calculated. It is assumed that the flue gas leaves the burning surface, perpendicularly, with velocity. Thus, radial and tangentional flue gas velocities, adjacent to the propellant, are given as[3]:

$$u = v_s \mathrm{Sin}(\theta_c - \theta), \quad w = v_s \mathrm{Cos}(\theta_c - \theta) \qquad \ldots (21)$$

The continuity and incompressible Euler equations for the element, illustrated in Fig. 5, are written for an irrotational flow, along two axis, shown in Fig. 6. By employing a convenient transfer matrix, equations are transferred into the coordinates, as given in Fig. 4(b).

Flow velocities are calculated by solving achieved sets of equations, as follows:

$$\frac{\partial V_r}{\partial r} + \frac{\partial V_z}{\partial z} + \frac{1}{r}V_r = 0 \qquad \ldots (22)$$

$$V_r\frac{\partial V_r}{\partial r} + V_z\frac{\partial V_z}{\partial z} = -\frac{1}{\rho}\frac{\partial P}{\partial r} \qquad \ldots (23)$$

$$V_r\frac{\partial V_z}{\partial r} + V_z\frac{\partial V_z}{\partial z} = -\frac{1}{\rho}\frac{\partial P}{\partial z} \qquad \ldots (24)$$

Having calculated velocities, Nusselt number and convection heat transfer coefficient are determined.

4.0 TEST PROCEDURE

A double base solid propellant with 30mm outside diameter is employed for all the tests. Tests of the foil embedded solid propellant were designed and executed in two following categories:

1) Atmospheric tests

2) Static tests in a model motor

https://doi.org/10.1017/S0001924000002694 Published online by Cambridge University Press

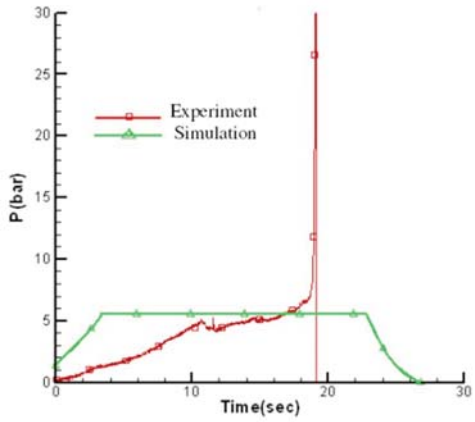


Figure 8. Sample of static test and internal ballistic program results (AL, 50μ).

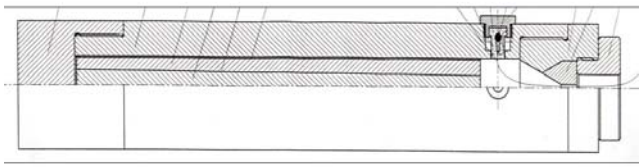


Figure 9. Sectional drawing of the motor.

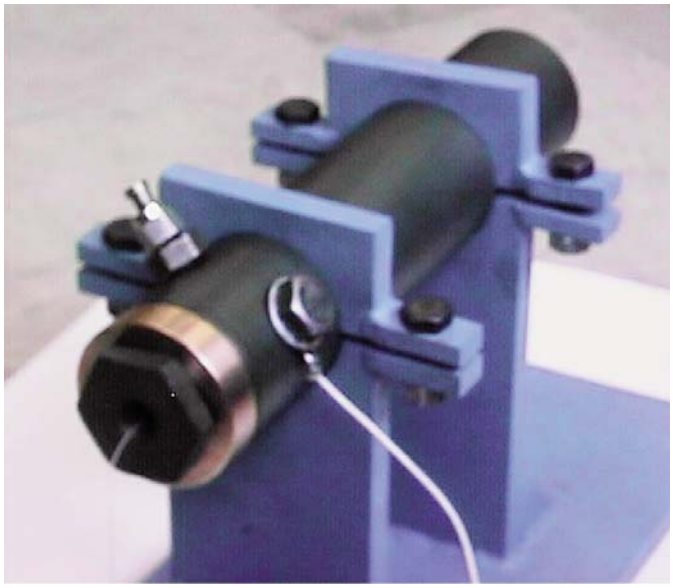


Figure 10. Solid propellant motor on fixture.



Figure 11. Fixed and changeable nozzles.

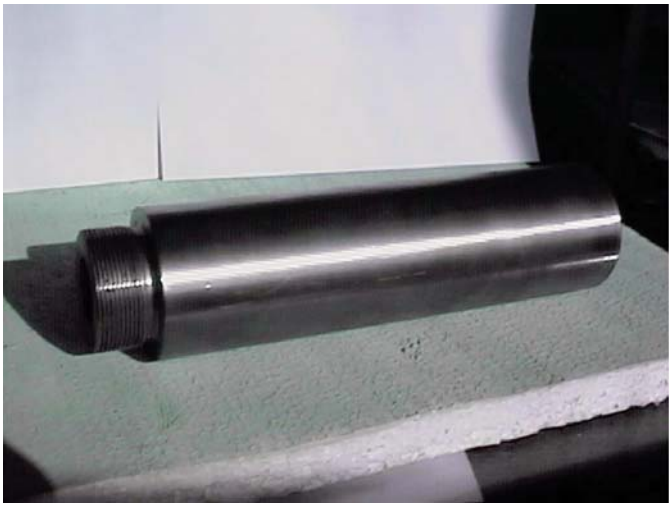


Figure 12. Motor tube.

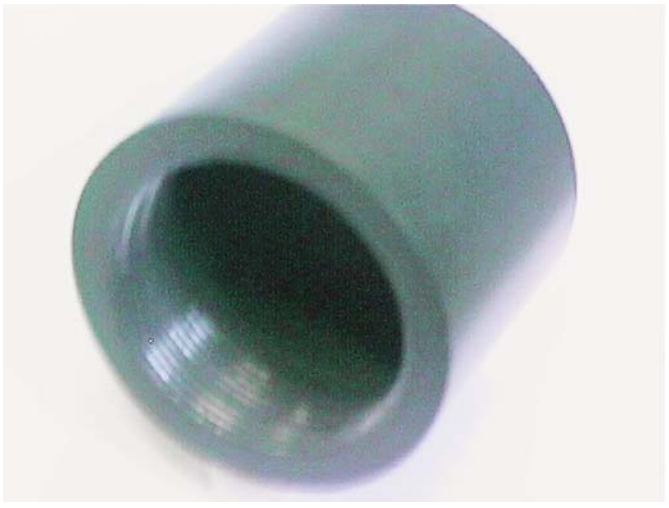


Figure 13. Adaptor.

https://doi.org/10.1017/S0001924000002694 Published online by Cambridge University Press

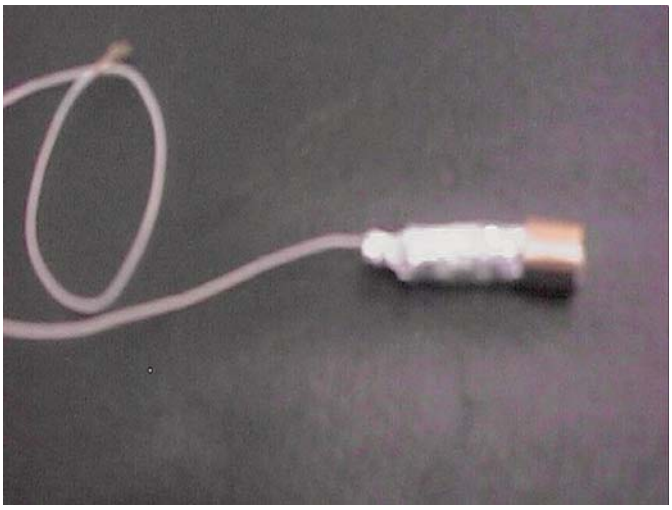


Figure 14. Igniter.

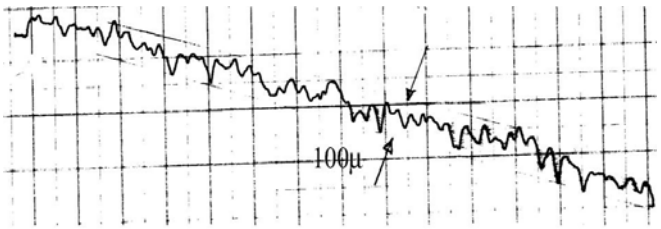


Figure 15. Propellant surface measured by contour-graph.

The main aims of the atmospheric tests were observing the foil embedded combustion, investigating the W-shape formation, and studying the cone angle.

Through the static tests, embedded solid propellant combustion is examined by implementing a model solid propellant motor. Based on these tests, pressure-time curves are drawn and compared with computational results.

The cross-sections of the burned propellants, embedded with 50 microns aluminium and copper foils, are shown in Fig. 7. Solid propellant length and diameter are 220mm and 30mm, respectively, and the metallic foil is embedded in the middle of the solid propellant.

In Fig. 8 samples of experimental and simulation results are shown for a solid propellant, embedded with 50 microns aluminium foil. The experimental result corresponds to an explosion at the end, which will be explained later.

To perform static tests on foil embedded solid propellants and to provide pressure-time curves, one small size motor with a high range of safety factor was designed and manufactured, so that execution of several static tests was rezndered possible (Fig. 9). In addition, for fixing the motor during the tests, one fixture is fabricated. The complete motor, installed on the fixture, is shown in Fig. 10. In order to perform tests with various throttle diameters, one motor tube, twenty changeable nozzles, and one adaptor were designed and manufactured (Figs 11, 12 and 13).

Parallel to the aforesaid activities, to achieve 30 ~ 40% of maximum combustion pressure and to ignite the propellant, the igniter is designed based on characteristics of black powder (Fig. 14).

It is worthwhile to mention that the surfaces of the inner and outer propellants are machined, precisely, and after inserting the foil, they are attached to each other by Patex glue. However, as shown in Fig. 15, the propellant surface may not be quite smooth, and roughness up to 100 microns may appear. In this case, the flue gas penetrates into the gap, between the propellant and foil, which increases drastically the burning surface. As a result, the pressure inside the motor increases suddenly, which may lead to an explosion (Fig. 8).

5.0 TEST RESULTS

During this research 17 atmospheric tests and 15 static tests were programmed and executed. Aluminium foils with thicknesses of 25, 50, 100, and 150 microns and copper foils with thicknesses of 50, 100, 150 and 200 microns were utilised. By applying atmospheric tests, θ values are obtained, and based on static tests, N values are derived for different thicknesses of aluminium and copper foils. In Fig. 16 experimental results for 'θ' are shown for various aluminium foil thicknesses. It can be seen that by increasing the aluminium foil thickness up to 150 microns, 'θ' decreases and, consequently, N increases. In other words, by thickening the aluminium foil, burning surface increases and burning time decreases. In Fig. 17 experimental results for 'θ' are shown for diverse copper foil thicknesses. For this case, the behaviour of the curve is quite different. It is revealed that as copper foil thickness augments up to 120 microns, 'θ' decreases, and for larger thicknesses, 'θ' increases. For wire embedding, Rumbel[1] and Kubota[6] have, likewise, reported that there is an optimum wire diameter for which 'θ' is minimum and combustion surface is maximum. For copper foil, the optimum value of 'θ' appears at the thickness of 120 microns.

In general, since the thermal diffusivity of copper is higher than that of aluminium, 'θ' is smaller for copper foil than for aluminium foil. It can be concluded that it is possible to increase burning rate and motor thrust more easily, by using copper foils rather than aluminium foils. Furthermore, copper has higher melting temperature than aluminium. So, the portion of aluminium foil, adjacent to the hot gas, melts rapidly, but copper can resist against higher temperatures and can intensify the heat penetration into the propellant. According to the propellant manufacturer the burning parameters for the tested propellant (without embedded foil) are: $a = 1{\cdot}5\text{m}^{s}$ and $n = 0{\cdot}4$.

Figure 18 shows the comparison between variation of 'N' for copper wire embedding, concluded by King[2], and copper foil embedding. It can be seen that for the thicknesses between 90 up to 180 microns, foil embedding is more efficient than wire embedding.

Figure 19 compares the variation of 'N' regarding foil thickness for aluminium and copper. Hence, copper foil increases the burning surface more than aluminium foil. This feature is shown in Fig. 20, in which burning surface is drawn based on foil thickness for aluminium and copper.

Burning rates along the embedded foil, concluded from test results, are shown in Fig. 21, for copper and aluminium foils. Comparing the burning rate of end-burning propellant (1·5mm/s), with those of embedded propellants with metallic foils, it can be confirmed that foil embedding may improve burning rate. Moreover, for the tested thicknesses, copper foil increases the burning rate more than aluminium foil.

https://doi.org/10.1017/S0001924000002694 Published online by Cambridge University Press

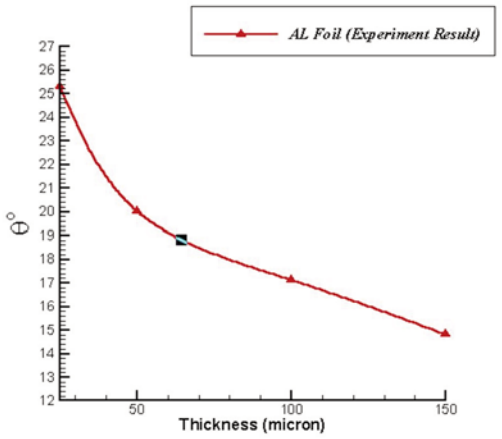


Figure 16. Experimental results for various aluminium foil thicknesses.

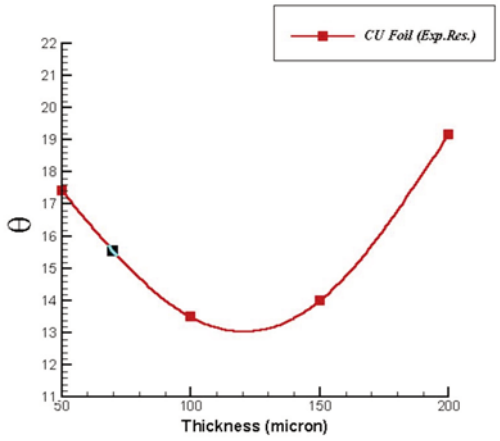


Figure 17. Experimental results for various copper foil thicknesses.

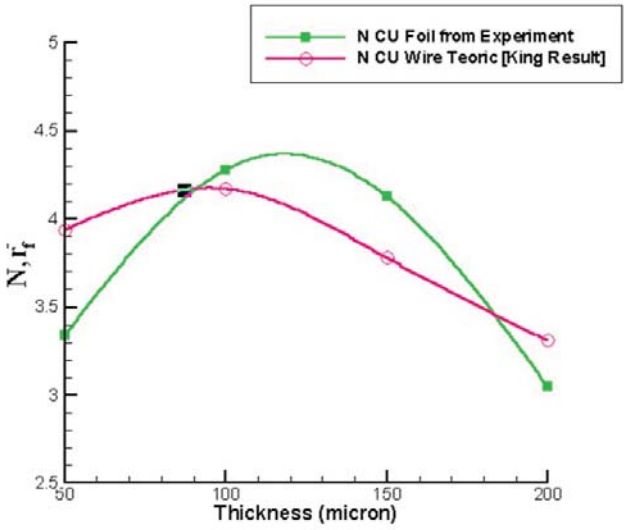


Figure 18. Comparison of experimental results with results of King *et al*[2].

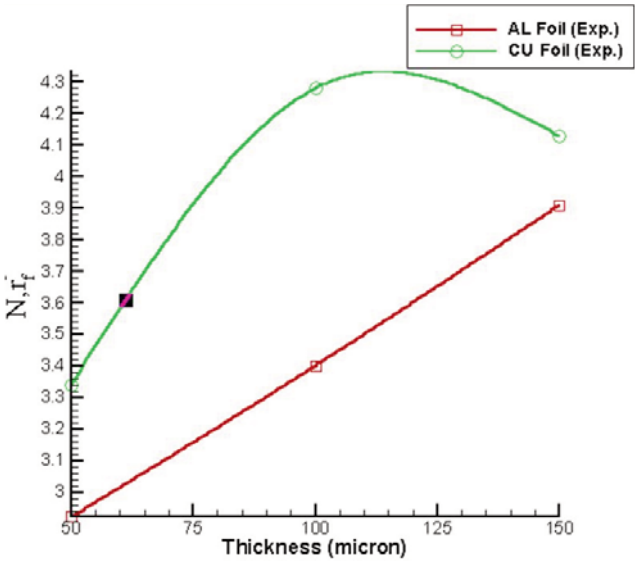


Figure 19. Experimental results comparison for copper and aluminium foils.

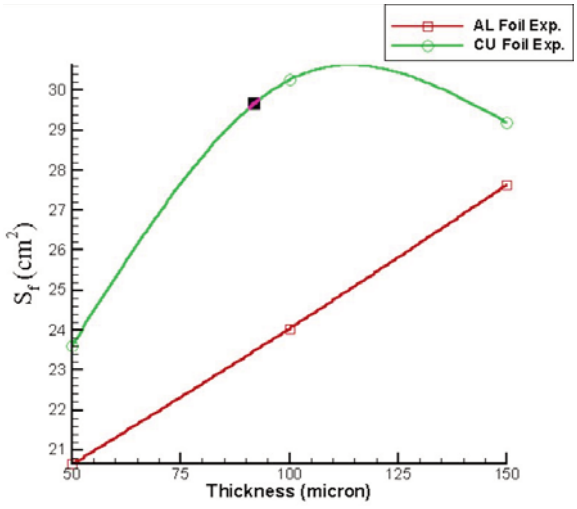


Figure 20. Comparison of burning surfaces for copper and aluminium foils.

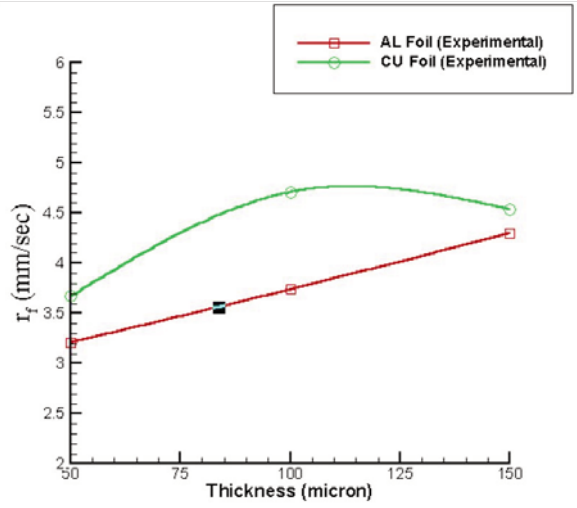


Figure 21. Comparison of burning rates for copper and aluminium foils.

https://doi.org/10.1017/S0001924000002694 Published online by Cambridge University Press

6.0 CONCLUSIONS

In this investigation a novel method of cylindrical foil embedding is selected and applied to double base solid propellant. It is shown that by using the foil embedding method, the burning characteristics of solid propellants can be improved, and burning time can be decreased regarding end-burning. In addition, a complete data bank, including burning rate parameters are obtained for foil embedded double base solid propellants.

Accordingly, in propulsion motors, liquid fuels may be replaced with solid propellants, for which burning times are conveniently modified and adjusted by using the foil embedding method.

7.0 REFERENCES

1. RUMBEL, K.E., COHEN, M., HENDERSON, C.B. and SCURLOCK, A.C. A physical means of attaining high burning rate in solid propellants Eleventh Army-Navy-Air force Solid Propellant Meeting, Washington DC, USA, May 1955, p 155.
2. KING, M.K. Analytical modelling of effects of wires on solid motor ballistics, *J Propulsion*, May-June 1991, **7**, (3).
3. GOHARI, H. and SERAJ MEHDIZADEH, N. Experimental Investigation of Foil Embedding Effect on Solid Propellant Burning, M.Sc. Thesis, February 2001, Amirkabir University of Technology, Iran.
4. SAHAFIYAN, A. and AFSHANI, M.E. Performance simulation of a dual thrust rocket motor International, Autumn Seminar on Propellants, *Explosives and Pyrotechnics*, **1**, 2005, p 547, Beijing Institute of Technology, Beijing, China.
5. CAVENY, L.H. and GLICK, R.L. Influence of embedded metal fibers on solid propellant burning rate, *J Spacecraft and Rockets*, January 1967, **4**, p 79.
6. KUBOTA, N., ICHIDA, M. and FUJISAWA, T. Combustion processes of propellants with embedded metal wires, AIAA, January 1982, p 116, **20**.

https://doi.org/10.1017/S0001924000002694 Published online by Cambridge University Press